New Identification of the Mixed-Morphology Supernova Remnant G298.6−0.0 with Possible Gamma-ray Association

Aya BAMBA[1], Makoto SAWADA[1], Yuto NAKANO[1], Yukikatsu TERADA[2], John HEWITT[3,4], Robert PETRE[3], Lorella ANGELINI[3],

[1] Department of Physics and Mathematics, Aoyama Gakuin University, 5-10-1 Fuchinobe Chuo-ku, Sagamihara, Kanagawa, 252-5258, Japan

[2] Department of Physics, Science, Saitama University, Sakura, Saitama 338-8570, Japan

[3] NASA Goddard Space Flight Center, Greenbelt, MD 20771, USA

[4] Center for Research and Exploration in Space Science and Technology (CRESST), University of Maryland, Baltimore County, Baltimore, MD 21250, USA

Received ; Accepted

Abstract

We present an X-ray analysis on the Galactic supernova remnant (SNR) G298.6−0.0 with Suzaku. The X-ray image shows a center-filled structure inside the radio shell, implying this SNR is categorized as a mixed-morphology (MM) SNR. The spectrum is well reproduced by a single temperature plasma model in ionization equilibrium, with a temperature of 0.78 (0.70–0.87) keV. The total plasma mass of 30 $M_{\odot}$ indicates that the plasma has interstellar medium origin. The association with a GeV gamma-ray source 3FGL J1214.0−6236 on the shell of the SNR is discussed, in comparison with other MM SNRs with GeV gamma-ray associations. It is found that the flux ratio between absorption-corrected thermal X-rays and GeV gamma-rays decreases as the MM SNRs evolve to larger physical sizes. The absorption-corrected X-ray flux of G298.6−0.0 and the GeV gamma-ray flux of 3FGL J1214.0−6236 closely follow this trend, implying that 3FGL J1214.0−6236 is likely to be the GeV counterpart of G298.6−0.0.

Key words: ISM: supernova remnants — ISM: individual (G298.6−0.0) — X-rays: ISM — gamma-rays:

1 Introduction

The origin of Galactic cosmic rays has remained an unresolved question since their discovery. One of the most plausible acceleration sites is at the shock front of supernova remnants (SNRs). The discovery of synchrotron X-rays (Koyama et al. 1995) and very high energy (VHE) gamma-rays (Aharonian et al. 2004) from shells of SNRs gave some of the first clear evidence of active particle acceleration in these shocks. The small-scale structure and time variability of synchrotron X-rays imply that the acceleration is very efficient (Bamba et al. 2003; Bamba et al. 2005; Uchiyama et al. 2007). However, it remains an open question how accelerated particles escape from the shocks to become cosmic rays.

Recently, Fermi detected GeV gamma-rays from several SNRs (Abdo et al. 2010a; Abdo et al. 2010b; Abdo et al. 2010c). Interestingly, many of the GeV-detected SNRs are many times older than the non-thermal X-ray-detected or VHE-gamma-ray-detected SNRs (Funk 2011). Moreover, their GeV spectra are soft and show a spectral break at energies around 1–10 GeV, implying that high energy particles have already lost their energy or have escaped from the acceleration sites. If the latter is true, their soft spectra show the evidence of particle escape. However, a larger sample of GeV gamma-ray SNRs is needed to judge the particle escape scenario.

We searched for GeV gamma-ray sources associated with cataloged Galactic SNRs in the Fermi Large Area Telescope Third Source Catalog (The Fermi-LAT Collaboration 2015). There are 60 GeV gamma-ray sources which spatially coincide with the Galactic SNRs, in addition to the 12 SNRs identified by extended gamma-ray emission. 3FGL J1214.0−6236 is associated with the radio SNR G298.6−0.0, detected at 408 MHz and 843 MHz with a flat radio spectral index of -0.3 (Shaver & Goss 1970; Kesteven & Caswell 1987; Whiteoak & Green 1996). Reach et al. (2006) reported a possible detection of infrared emission from the direction of G298.6−0.0, implying that the shock of this remnant may have encountered a high-density medium. These characteristics are common among GeV gamma-ray-emitting SNRs. However, no detection has been made in the X-ray band with ROSAT PSPC (Hwang & Markert 1994). X-ray information is critical to estimate the physical parameters of the SNR, such as age, explosion energy, and the amount of accelerated electrons. Thus, our aim is to identify X-rays from G298.6−0.0 and measure parameters using the low and stable background X-ray observations provided by Suzaku (Mitsuda et al. 2007).

In this paper, we report the first X-ray imaging spectroscopy of G298.6−0.0 using Suzaku. The observation details are summarized in §2. An analysis of the Suzaku X-ray data is presented in §3, the results of which are discussed in §4.

2 Observations and Data Reduction

Suzaku observed G298.6−0.0 on 2012, Aug. 11–13 (sequence number: 507037010) and 2013, Feb. 18–19 (sequence number: 507037020). Only three set of the onboard X-ray Imaging Spectrometers (XIS0, 1, 3; Koyama et al. 2007) could be used in this paper, due to a known problem with XIS2. XIS1 is a back-illuminated CCD, whereas the others are front-illuminated. The XIS instruments were operated in the normal-clocking full-frame mode. Spaced-row charge injection technique and the relevant energy calibration method were applied to mitigate the long-term degradation of the energy resolution (Uchiyama et al. 2009). Since the observing mode is the same for the two observations, we analyzed the combined data using HEADAS software version 6.16 and XSPEC version 12.8.2. We reprocessed the data set with the calibration database version 2012-11-06 for XIS and 2011-06-30 for X-ray Telescope (XRT; Serlemitsos et al. 2007).

In the XIS data screening, we filtered out data acquired during passages through the South Atlantic Anomaly (SAA), with elevation angles with respect to the Earth's dark limb below 5 deg, or with elevation angle to the bright limb below 20 deg in order to avoid contamination by emission from the bright limb. The remaining exposure is 57 ks (17 ks for the former observation and 40 ks for the latter observation).

3 Results

3.1 Images

Figure 1 (a) shows 843 MHz (Whiteoak & Green 1996) and the XIS 1+3 0.5–5 keV band images of G298.6−0.0 region. XIS 0 image is not used due to the dead column. The position of the Fermi source, 3FGL J1214.0−6236, is also shown. The radio emission shows the clear shell-like structure, while X-ray emission has a center-filled morphology inside the radio shell and does not show any prominent point sources. These results show that G298.6−0.0 is either a SNR with a central pulsar or a mixed-morphology SNR (MM SNR; Rho & Petre 1998). The point source located in the north-east of the SNR is coincident with the ROSAT source 1RXS J121248.7−623027 (Fuhrmeister & Schmitt 2003) and categorized as a rotationally variable star (Kiraga 2012), whose details are out of the scope of this paper.

3.2 Spectra

The source spectra of G298.6−0.0 were extracted from circular region with the radius of 3.9 arcmin, whereas the background spectra were taken from the source free region, as shown in Figure 1 (b). We added XIS0 and XIS3 spectra for the better statistics, whereas XIS1 spectrum was treated separately due to the different response from the others.

Background-subtracted spectra are shown in Figure 2. The spectra are rather soft and have emission lines, implying that the emission has a thermal origin. We thus adopted an optically thin thermal plasma model in collisional ionization equilibrium (VAPEC) affected by interstellar absorption (PHABS; Balucinska-Church & McCammon 1992). For both the emission and absorption models, the solar abundance values of Anders & Grevesse (1989) were used. The first fit with fixed abundances at the solar values was rejected with the reduced χ^2 of 228.6/117 and wavy residuals. We thus fit with the abundances of Mg, Si, S, and Fe as free parameters. This improved fit gave a reduced χ^2 of 136.1/113. The best-fit models and parameters are shown in Figure 2 and Table 1, respectively. We also tried to fit with non-equilibrium ionization plasma models, VNEI for ionizing plasma and VVRNEI for recombining plasma. The abundances of Mg, Si, S, and Fe were treated as free parameters. For a VVRNEI model, we fixed the initial plasma temperature to be 3 keV. The fitting showed similar reduced χ^2 of 136.5/112 (VNEI) and 131.5/112 (VVRNEI). The best-fit values of the ionization/recombination timescale are $> 9.8 \times 10^{11}$ cm^{-3}s for the VNEI model and 6.2 (5.3–14) $\times 10^{11}$ cm^{-3}s for the VVRNEI model, respectively. The latter gives a slightly shorter relaxation timescale than that in ionization equilibrium (10^{12-13} s cm^{-3}). However, the improvement of the fit is only marginal; both models show similar reduced χ^2. Moreover, there is no clear indication of strong radiative recombination continuum in the residual which is the direct evidence of a recombining plasma (Yamaguchi et al. 2009). Thus we concluded that the plasma is well described by an absorbed plasma emission model in ionization equilibrium. We note that the XIS1 spectrum has residuals in the low energy band, which may be due to the calibration uncertainty of contamination.

4 Discussion

4.1 Physical Parameters of G298.6−0.0

We report the first detection of thermal X-rays from inside the radio SNR G298.6−0.0. The characteristics of G298.6−0.0 classify it as a new MM SNR. Here, we estimate several physical parameters for this SNR.

First, we estimate the distance to this source. We measured the absorption column to the source to be $1.65\ (1.45 - 1.99) \times 10^{22}$ cm^{-2}. The total hydrogen density throughout the Galaxy in

this direction is estimated by the method of Willingale et al. (2013). The $\mathrm{H_I}$ column density in this direction is 1.4 $\times 10^{22}$ atoms cm^{-2} (Kalberla et al. 2005), whereas the column density of molecular hydrogen ($\mathrm{H_2}$) is 1.4$\times 10^{21}$ atoms cm^{-2} from the dust map (Schlegel et al. 1998). The total absorption column is thus 1.5$\times 10^{22}$ atoms cm^{-2}, which is similar value to our target. This indicates that the SNR is located in the outer part of the Galaxy. According to the face-on map by Nakanishi & Sofue (2006), most of the interstellar hydrogens in this direction are located within 10 kpc from the Sun. Thus we adopt the distance of 10 kpc. This is an independent constraint from that indicated by the $\Sigma - D$ relation in the radio band (9.5 kpc; Case & Bhattacharya 1998). The previous method only gives a rough estimate and more detailed studies are necessary to get a better measurement of the distance to SNR G298.6−0.0.

Assuming the plasma fills a 3.9 arcmin sphere, the total volume is $1.8\times 10^{59} D_{10}^3$ cm^3, where D_{10} is the distance in the unit of 10 kpc. The average density derived from the emission measure (Table 1) is $0.2 D_{10}^{-1/2} f^{1/2}$ cm^{-3}, where f is the filling factor. The total mass and thermal energy can be estimated as $30 D_{10}^{5/2} f^{1/2} M_\odot$ and $6.4 \times 10^{49} D_{10}^{5/2} f^{1/2}$ erg, respectively. The large total mass indicates that the main component of the plasma originates from swept-up interstellar medium.

4.2 Comparison with other SNRs with GeV counterpart

Here, we discuss on the comparison with G298.6−0.0 and other MM SNRs with GeV gamma rays, to judge whether 3FGL J1214−6236 has similar properties to other GeV counterparts of MM SNRs.

GeV emission is coincident with the shell of G298.6−0.0, which is same to other SNR cases (Abdo et al. 2010a). The possible interaction with a high-density medium from the direction of this SNR is reported (Reach et al. 2006), which is also similar to other GeV SNR samples. On the other hand, we have no information which part of this SNR interacts with high-density medium. Further studies in infrared or molecular cloud bands is needed to conclude the interaction. The GeV spectrum of 3FGL J1214.0−6236 has a spectral break around a few GeV (The Fermi-LAT Collaboration 2015), which is also similar to the spectra of other GeV SNRs. These facts imply that 3FGL J1214.0−6236 is a possible GeV counterpart of G298.6−0.0.

Table 2 shows the summary of the properties across the absorption-corrected 0.3–10 keV and 0.1–100 GeV bands of the GeV gamma-ray emitting MM SNRs. Large distance uncertainties for these sources make it difficult to apply a detailed model of the X-ray and GeV gamma-ray evolution to the case of G298.6−0.0. Instead we compare the flux ratio between absorption-corrected X-rays and GeV gamma-rays, which is independent from the distance.

We selected samples with known total absorption-corrected X-ray and GeV gamma-ray fluxes.

Recent studies revealed that some of our samples have X-ray emission from recombining plasma with detailed analysis (Ozawa et al. 2009; Uchida et al. 2012; Sato et al. 2014), but we concentrate on total X-ray flux from older results as it is an easy comparison for the other fainter sources. IC443 is a famous MM SNRs with GeV gamma-rays (Yamaguchi et al. 2009; Abdo et al. 2010c), but do not have a good estimate of the total X-ray flux in the literatures due to their large apparent diameters, and thus we did not adopt it as our samples. We also ignored emission from ejecta reported in W49B and G349.7+0.2 (Kawasaki et al. 2005; Yasumi et al. 2014), which contributes only $\sim$10% flux of the total flux. GeV gamma-ray spectra for several sources have spectral breaks around 10 GeV (Abdo et al. 2010a; Abdo et al. 2010b; Abdo et al. 2010c, for example). To treat fainter sources equally, we used the total energy flux from the Fermi source catalog (The Fermi-LAT Collaboration 2015). The difference in the fluxes of W44 between the catalog and that derived by Abdo et al. (2010a) is only about 20%, which is negligible for our study. We estimated the radii using the catalog of Galactic SNRs by Green (2014).

The flux ratio between 0.3–10 keV and 0.1–100 GeV, F_X/F_G in Table 2, is in the range of $\sim$0.1–30. If 3FGL J1214.0$-$6236 is the gamma-ray counterpart of G298.6$-$0.0, our target has the faintest F_X/F_G ratio. Figure 3(a) shows the radius vs. F_X/F_G of MM SNRs with GeV gamma-rays. The flux ratio shows decline as the radii of SNRs is larger, or SNRs evolves older. The flux ratio of our target is well consistent with this trend.

It is unclear why the flux ratio becomes smaller when MM SNRs evolve. One possibility is that the X-ray luminosity decreases faster due to the expansion and cooling (Gehrels & Williams 1993), whereas the GeV gamma-ray luminosity does not decrease. In order to check this hypothesis, we have made plots of radius vs. 0.3–10 keV luminosity (Figure 3(b)) or 0.1–100 GeV luminosity (Figure 3(c)). This is consistent with our scenario; The X-ray luminosity become smaller when SNRs evolve (or radii become larger), whereas the gamma-ray luminosity is almost constant in the range of 10^{35}–10^{36} erg s^{-1}. This is also consistent with previous results in X-rays (Long 1983) and GeV gamma-rays (Brandt et al. 2015). The constant gamma-ray flux support our hypothesis that timescale for low-energy particles to escape these SNRs is long in comparison to the SNR evolution. This trend also implies that a part of Galactic GeV unID sources can be very evolved MM SNRs without significant detection in X-ray and radio bands. Note that radio surface brightness becomes smaller when the SNR evolves (Case & Bhattacharya 1998), which makes difficult to detect them together with large angular size. Further study of a large sample of GeV gamma-ray SNRs is needed to understand this tendancy.

Acknowledgments

We thank the anonymous referee for the fruitful comments. This research has made use of the SIMBAD database, operated at CDS, Strasbourg, France. This work was supported in part by Grant-in-Aid for Scientific Research of the Japanese Ministry of Education, Culture, Sports, Science and Technology (MEXT) of Japan, No. 22684012 and 15K05107 (A. B.) and No. 15K17657 (M. S.).

References

Abdo, A. A., Ackermann, M., Ajello, M., et al. 2010a, Science, 327, 1103

Abdo, A. A., Ackermann, M., Ajello, M., et al. 2010b, ApJ, 718, 348

Abdo, A. A., Ackermann, M., Ajello, M., et al. 2010c, ApJ, 712, 459

Aharonian, F. A., Akhperjanian, A. G., Aye, K.-M., et al. 2004, Nature, 432, 75

Anders, E., & Grevesse, N. 1989, Geochim. Cosmochim. Acta, 53, 197

Balucinska-Church, M., & McCammon, D. 1992, ApJ, 400, 699

Bamba, A., Yamazaki, R., Ueno, M., & Koyama, K. 2003, ApJ, 589, 827

Bamba, A., Yamazaki, R., Yoshida, T., Terasawa, T., & Koyama, K. 2005, ApJ, 621, 793

Brandt, T. J., Acero, F., de Palma, F., et al. 2015, arXiv:1507.03633

Case, G. L., & Bhattacharya, D. 1998, ApJ, 504, 761

Claussen, M. J., Frail, D. A., Goss, W. M., & Gaume, R. A. 1997, ApJ, 489, 143

Clemens, D. P. 1985, ApJ, 295, 422

The Fermi-LAT Collaboration 2015, ApJS, in print, arXiv:1501.02003

Fuhrmeister, B., & Schmitt, J. H. M. M. 2003, A&A, 403, 247

Funk, S. 2011, talk in TeV particle Astrophysics 2011 AlbaNova University center, Sweden

Gehrels, N., & Williams, E. D. 1993, ApJL, 418, L25

Green, D. A. 2014, Bulletin of the Astronomical Society of India, 42, 47

Hwang, U., & Markert, T. H. 1994, ApJ, 431, 819

Kalberla, P. M. W., Burton, W. B., Hartmann, D., et al. 2005, A&A, 440, 775

Kawasaki, M., Ozaki, M., Nagase, F., Inoue, H., & Petre, R. 2005, ApJ, 631, 935

Kesteven, M. J., & Caswell, J. L. 1987, A&A, 183, 118

Kiraga, M. 2012, Acta. Astron., 62, 67

Koyama, K., Petre, R., Gotthelf, E. V., et al. 1995, Nature, 378, 255

Koyama, K., Tsunemi, H., Dotani, T., et al. 2007, PASJ, 59, 23

Long, K. S. 1983, Suprenova Remnants and their X-ray Emission, 101, 525

Tian, W. W., & Leahy, D. A. 2014, ApJL, 783, L2

Mitsuda, K., Bautz, M., Inoue, H., et al. 2007, PASJ, 59, 1

Table 1. Best-fit parameters of the spectral fitting (VAPEC)[†].

Parameters	Values
$N_{\rm H}$ (10^{22} cm^{-2})	1.65 (1.45–1.99)
kT (keV)	0.78 (0.70–0.87)
Mg	0.59 (0.39–0.86)
Si	0.38 (0.27–0.50)
S	0.35 (0.21–0.50)
Fe	$<$0.23
$E.M.$[‡]	5.6 (4.1–8.1)
reduced χ^2	136.1/113

[†]: Errors indicate single parameter 90% confidence interval.

[‡]: Emission measure in the unit of $\frac{10^{-11}}{4\pi D^2}\int n_e n_H dV \,\mathrm{cm}^{-5}$, where D, n_e, and n_H represent the distance, and electron and hydrogen densities.

Nakanishi, H., & Sofue, Y. 2006, PASJ, 58, 847

Ozawa, M., Koyama, K., Yamaguchi, H., Masai, K., & Tamagawa, T. 2009, ApJL, 706, L71

Radhakrishnan, V., Goss, W. M., Murray, J. D., & Brooks, J. W. 1972, ApJS, 24, 49

Reach, W. T., Rho, J., Tappe, A., et al. 2006, AJ, 131, 1479

Rho, J., & Petre, R. 1998, ApJL, 503, L167

Rho, J., & Borkowski, K. J. 2002, ApJ, 575, 201

Sato, T., Koyama, K., Takahashi, T., Odaka, H., & Nakashima, S. 2014, PASJ, 66, 124

Schlegel, D. J., Finkbeiner, D. P., & Davis, M. 1998, ApJ, 500, 525

Serlemitsos, P. J., Soong, Y., Chan, K.-W., et al. 2007, PASJ, 59, 9

Shaver, P. A., & Goss, W. M. 1970, Australian Journal of Physics Astrophysical Supplement, 14, 133

Uchida, H., Koyama, K., Yamaguchi, H., et al. 2012, PASJ, 64, 141

Uchiyama, H., Ozawa, M., Matsumoto, H., et al. 2009, PASJ, 61, 9

Uchiyama, Y., Aharonian, F. A., Tanaka, T., Takahashi, T., & Maeda, Y. 2007, Nature, 449, 576

Whiteoak, J. B. Z., & Green, A. J. 1996, A&AS, 118, 329

Willingale, R., Starling, R. L. C., Beardmore, A. P., Tanvir, N. R., & O'Brien, P. T. 2013, MNRAS, 431, 394

Yamaguchi, H., Ozawa, M., Koyama, K., et al. 2009, ApJL, 705, L6

Yasumi, M., Nobukawa, M., Nakashima, S., et al. 2014, PASJ, 66, 68

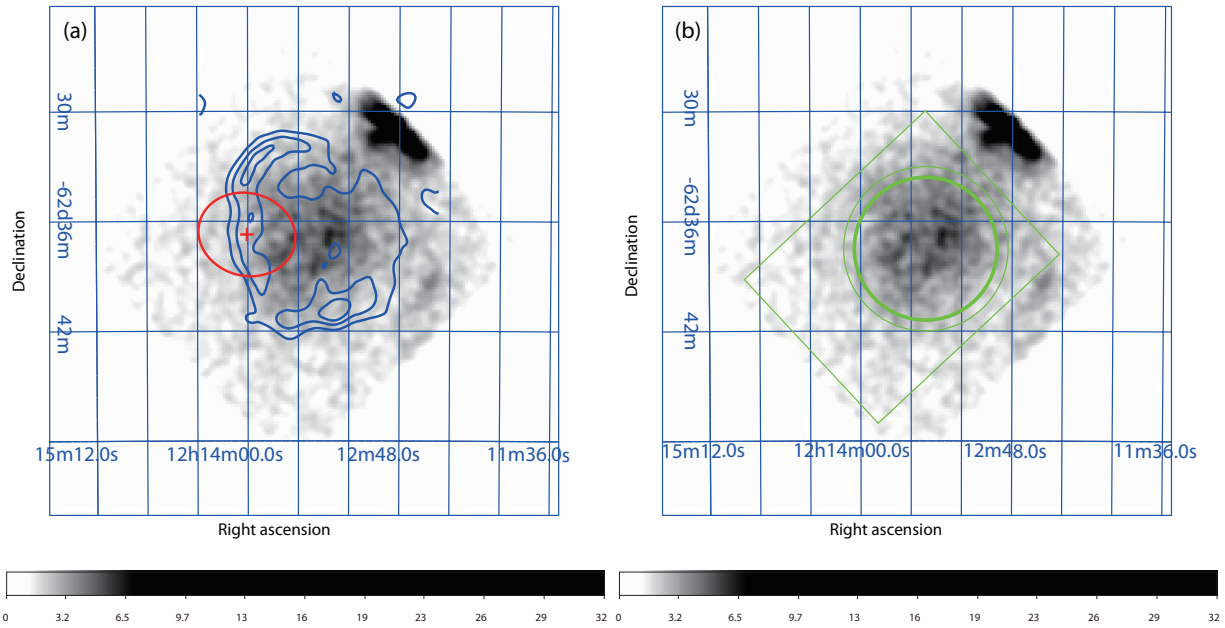

Fig. 1. (a): The 843 MHz (contours) and 0.5–5 keV (gray scale) images of the G298.6−0.0 region. The X-ray image is smoothed with a Gaussian function with the kernel of 0.4 arcmin, Non–X-ray background (NXB) was not subtracted, and no vignetting correction was performed. The color scale is in logarithmic scale. Red circle shows the error region of the Fermi source 3FGL J1214.0−6236. The coordinate is in J2000. The point source in the north-west is 1RXS J121248.7−623027 (Fuhrmeister & Schmitt 2003). (b): Same image to (a) with source (bold) and background (thin) regions for the spectral analysis.

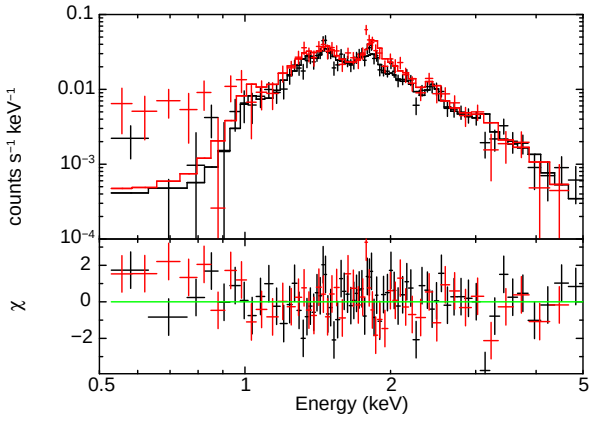

Fig. 2. Background-subtracted spectra of the source region. Black and red closses represent FI and BI spectra, respectively. The solid lines represent the best-fit VAPEC model.

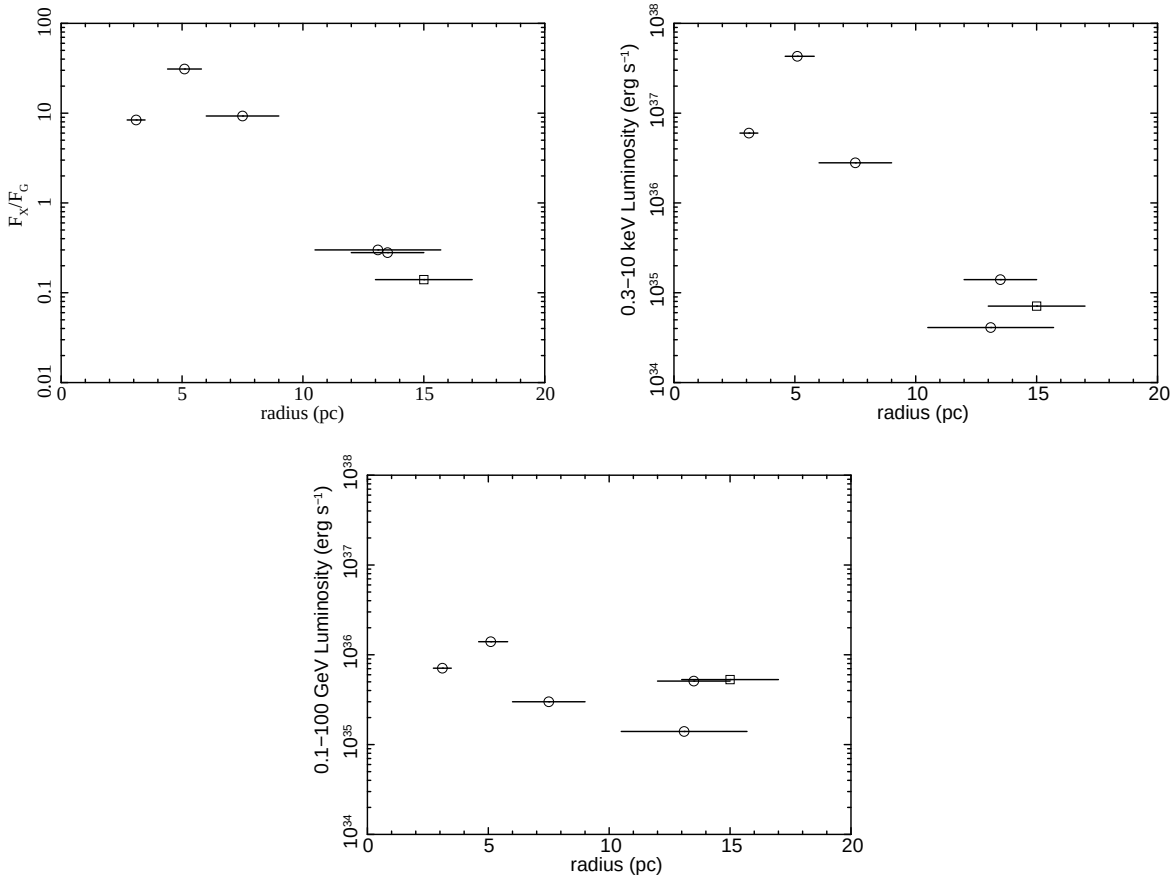

Fig. 3. (a): Radius vs. flux ratio between 0.3–10 keV (absorption-corrected, F_X) and 0.1–100 GeV (F_G) for MM SNRs with GeV gamma-ray emission. Circles and the box represent the samples from literatures and from this work, respectively, in all panels. (b): Radius vs. 0.3–10 keV luminosity. (c): Radius vs. 0.1–100 GeV luminosity.

Table 2. X-ray and gamma-ray fluxes of MM SNRs with associations to GeV gamma-rays

Sample	D^a	Radius^b	$F_X{}^c$	$F_G{}^d$	F_X/F_G	References
W 49B	8	5.1 ± 0.7	56^e	1.8	31	(1) (2) (3)
G349.7+0.2 . .	11	3.0 ± 0.4	4.1^e	0.49	8.4	(4) (5) (3)
3C 391	7.2	7.5 ± 1.5	4.5	0.49	9.3	(6) (2) (3)
W28	1.8	13.1 ± 2.6	1.1^f	3.6	0.30	(7) (8) (3)
W 44	2.8	13.5 ± 1.5	1.5^f	5.4	0.28	(1) (2) (3)
G298.6+0.0 . .	10	15 ± 2	0.059	0.44	0.14	this work, (3)

Note — (1) Claussen et al. (1997), (2) Kawasaki et al. (2005), (3) The Fermi-LAT Collaboration (2015), (4) Tian & Leahy (2014),(5) Yasumi et al. (2014), (6) Radhakrishnan et al. (1972), (7) Clemens (1985), (8) Rho & Borkowski (2002)

^{a}:Distance to the source in the unit of kpc.

^{b}: In units of pc. Errors indicate the radii along the major and minor axes.

^{c}: absorption-corrected 0.3–10 keV flux in units of 10^{-10} erg cm^{-2}s^{-1}.

^{d}: 0.1–100 GeV flux in units of 10^{-10} erg cm^{-2}s^{-1}.

^{e}: Only ISM component was considered.

^{f}: The X-ray flux was not extracted from the entire SNR but from the brightest central regions.